

A TECHNIQUE FOR DETECTING STARLIGHT SCATTERED FROM TRANSITING EXTRASOLAR PLANETS WITH APPLICATION TO HD 209458B

XIN LIU, EDWIN L. TURNER
Princeton University Observatory, Princeton, NJ 08544, USA

NORIO NARITA, YASUSHI SUTO
Department of Physics, University of Tokyo, Tokyo 113-0033, Japan

JOSHUA N. WINN
Department of Physics, and Kavli Institute for Astrophysics and Space Research, Massachusetts Institute of Technology, Cambridge, MA 02139, USA

TORU YAMADA
Astronomical Institute, Tohoku University, Sendai 980-8578, Japan

BUN'EI SATO
Tokyo Institute of Technology, 2-12-1-S6-6, Ookayama, Meguro-ku, Tokyo 152-8550, Japan

WAKO AOKI, MOTOHIDE TAMURA
National Astronomical Observatory of Japan, 2-21-1 Osawa, Tokyo 181-8588, Japan
Submitted to ApJ on November 2

ABSTRACT

We present a new technique for detecting scattered starlight from transiting, close-orbiting extrasolar giant planets (CEGPs) that has the virtues of simplicity, robustness, linearity, and model-independence. Given a series of stellar spectra obtained over various phases of the planetary orbit, the goal is to measure the strength of the component scattered by the planet relative to the component coming directly from the star. We use two complementary strategies, both of which rely on the predictable Doppler shifts of both components and on combining the results from many spectral lines and many exposures. In the first strategy, we identify segments of the stellar spectrum that are free of direct absorption lines and add them after Doppler-shifting into the planetary frame. In the second strategy, we compare the distribution of equivalent-width ratios of the scattered and direct components. Both strategies are calibrated with a “null test” in which scrambled Doppler shifts are applied to the spectral segments. As an illustrative test case, we apply our technique to spectra of HD 209458 taken when the planet was near opposition (with orbital phases ranging from 11 to 34°, where 0° is at opposition), finding that the planet-to-star flux ratio is $(1.4 \pm 2.9) \times 10^{-4}$ in the wavelength range 554–681 nm. This corresponds to a geometric albedo of 0.8 ± 1.6 , assuming the phase function of a Lambert sphere. Although the result is not statistically significant, the achieved sensitivity and relatively small volume of data upon which it is based are very encouraging for future ground-based spectroscopic studies of scattered light from transiting CEGP systems.

Subject headings: planetary systems — stars: individual — (HD 209458) — techniques: spectroscopic

1. INTRODUCTION

The discovery of the first exoplanet orbiting an ordinary main sequence star, 51 Peg, a dozen years ago (Mayor & Queloz 1995) also revealed the first example of a largely unexpected but common class of astronomical objects, namely close-orbiting extrasolar giant planets (CEGPs). The discovery of the first transiting exoplanet system, HD 209458b also a CEGP (Henry et al. 2000; Mazeh et al. 2000; Charbonneau et al. 2000; Brown et al. 2001), a few years later allowed study of these enigmatic objects to move beyond orbital parameters and minimum masses. Although radial velocity, transit and microlensing techniques have made the study of exoplanets one of the most active

and exciting areas of astrophysics in recent years and have produced a wealth of additional major discoveries and important theoretical problems (Perryman 2000; Chauvin 2007), the effort to understand CEGPs remains central to the field.

The light of the primary star scattered from CEGPs reflects the nature (composition, clouds, energy balance, structure, motions *et cetera*) of their atmospheres (e.g., Seager & Sasselov 1998; Marley et al. 1999; Seager et al. 2000; Sudarsky et al. 2000, 2003; Burrows et al. 2005); its direct detection would thus test and discriminate among emerging models of CEGPs.

There have been previous attempts to detect scattered starlight from CEGPs against the much brighter direct light from the primary via high-resolution spec-

transiting searches for the scattered, and hence Doppler-shifted, stellar absorption lines (Charbonneau et al. 1999; Leigh et al. 2003, and references therein). The problem is very difficult because the expected contribution of the scattered light to the total light is of order 10^{-4} or less for known CEGPs. Due to both the very small amplitude of the expected signal and the unknown orbital inclination angle i for non-transiting systems, the methods so far employed rely on model-dependent assumptions to estimate prior distributions for planetary radii, orbital inclinations and the form of the phase function (Leigh et al. 2003). The advantage of such an approach is that it can be applied to the brightest (but non-transiting) CEGP systems that thus have the least photon noise. In other words and as is usually the case, relying on a prior model allows one to maximize purely statistical signal-to-noise (S/N) but at the price of increased systematic uncertainty. Two previously published methods (e.g. Charbonneau et al. 1999; Cameron et al. 1999) depend on a χ^2 minimization applied to the whole stellar spectrum, which is not an optimally sensitive method for this problem because it dilutes the detectability of the scattered lines (which carry the signal of interest) by considering the quality of the fit to the continuum regions.

The simplest example of the advantage of studying transiting CEGP systems is that measurement of the scattered light fraction allows direct determination of the albedo in isolation, and not merely in combination with the planet’s radius squared (which must be estimated from a theoretical model for non-transiting systems). The major advantage of studying non-transiting systems is that some of them are nearly two orders of magnitude brighter than the brightest transiting system, thus yielding far smaller photon statistics noise.

Here we propose a largely model-independent technique to detect the scattered stellar absorption lines in transiting CEGP systems. In this method, no assumptions concerning the form of the phase function, the planet’s radius, the orbital inclination *et cetera* are needed to measure the planet-to-star flux ratio and albedo. Rather, only physical parameters of the system measured via transit observations are required. Moreover, the technique maximizes sensitivity by concentrating only on those portions of the spectrum in which scattered stellar lines are known to be present (at some amplitude to be measured). As a practical “worked example” we apply this technique to *Subaru* HDS spectra of HD 209458. The required input physical parameters of the system and their relation to the expected scattered light signal are briefly reviewed in §2. In §3, we describe the technique in detail, and apply it to HD 209458b, using high precision optical spectra acquired on UT 2002 October 27, with the *Subaru* High Dispersion Spectrograph (HDS; Noguchi et al. 2002). Results are summarized in §4. Prospects for future studies are then examined based on these results.

2. INPUT PARAMETERS

Our technique utilizes known physical properties of the transiting CEGP system based on prior radial velocity and transit studies.

The planet’s velocity relative to the star at orbital phase ϕ is given by (see, e.g. Collier Cameron et al. 2002)

$$V_P(\phi) = K_P \cdot \sin 2\pi\phi, \quad (1)$$

where $\phi = (t - T_0)/P_{orb}$ is the orbital phase at time t , T_0 is the transit epoch, and P_{orb} is the orbital period. Its apparent radial-velocity amplitude K_P about the mass center of the system is

$$K_P = \frac{2\pi a}{P_{orb}} \frac{\sin i}{1 + q}, \quad (2)$$

where a is the orbital distance, i is the inclination and $q \equiv M_P/M_\star$ is the mass ratio. The values of a and i can be measured from radial-velocity and transit-photometry data, respectively.

If the planet is tidally locked, as expected for nearly all CEGPs, there will be no rotational broadening. Then the scattered spectra will be the Doppler-shifted stellar spectra, scaled by a factor of the planet-to-star flux ratio ϵ , which is usually decomposed as (Charbonneau et al. 1999; Cameron et al. 1999)

$$\epsilon(\alpha, \lambda) = p(\lambda)g(\alpha, \lambda) \frac{R_P^2}{a^2}, \quad (3)$$

where $p(\lambda)$ is the geometric albedo, and $g(\alpha, \lambda)$ is the phase function, with α being the phase angle which varies as $\cos\alpha = -\sin i \cos 2\pi\phi$. The value of R_P is also measured from transit-photometry data.

3. METHOD AND APPLICATION TO HD 209458B

3.1. Overview

The basic idea behind the method is that for any absorption line in the primary star’s spectrum we can precisely predict the wavelength of each line in the light scattered from the planet in each exposure; it is simply offset from the position of the stellar line by the Doppler shift due to the planet’s orbital motion relative to the primary, as projected onto the line of sight to the observer at the time of that exposure. The strength of the scattered line relative to the line in the primary’s spectrum is just the fractional contribution of the planet’s scattered light to the total light at that wavelength; in principle, this line strength gives a measure of the planet’s albedo at that wavelength and phase angle.

Of course, in practice, for known CEGP systems this fraction is expected to be of order 10^{-4} to 10^{-5} and any individual line is thus completely undetectable even in very high S/N spectra. Our technique is then simply to superimpose and combine pieces of the spectra at the expected wavelengths of the scattered lines over many lines and exposures to achieve sufficient S/N to allow a statistically significant detection. This can be done either 1) by simply summing small fragments of the spectra centered on these predicted locations or 2) by measuring the ratio of scattered absorption line equivalent-widths to the corresponding equivalent widths in the primary and then combining the ratios over lines and exposures. We employ both variations.

In an attempt to detect tiny fractional signals against a noisy background, it is obviously crucial to know the background rather precisely and to characterize its noise properties accurately. We do both by an “internal” procedure using the same spectra and same wavelength regions in which we search for the signal. Specifically, in addition to combining the spectral fragments defined by the expected wavelength positions of the scattered lines, we also carry out the same analysis but with the

Doppler shift assigned to each exposure “shuffled” randomly among the exposures. In this way we can produce a large number of *reference spectra* made up of the same spectral fragments taken from the same set of exposures but each lacking any scattered line contribution. By combining this ensemble of reference spectra we obtain an excellent estimator of both the background against which we must distinguish the scattered light signal and of all of its noise properties (including, for example, the collective effects of weak stellar lines that cannot be detected individually).

Finally, in order to calibrate and test the method, it is very useful to have mock or simulated data containing an artificially injected, and thus precisely known, signal and having realistic noise properties. This we also manufacture internally. The individual spectra of the system are shifted to the planet’s rest frame at each exposure, and then multiplied by some assumed planet-to-star flux ratio ϵ to produce a set of artificial planet scattered light spectra. These artificial spectra are then added back into the individual exposures. For example, if the original spectra contain some scattered light signal with a planet-to-star ratio ϵ_0 , then these artificially injected spectra should have scattered light with a planet-to-star ratio $\epsilon_1 = (\epsilon_0 + \epsilon)$. We can analyze the artificially injected spectra to obtain ϵ_1 and then subtract ϵ_0 from it to recover ϵ . Successful, or failed, recovery of this known artificial signal by application of the same technique provides a strong test of the reliability and sensitivity of the method.

3.2. Data Preprocessing

As an illustrative case study, we analyze 33 Subaru HDS spectra of the system HD 209458, taken on UT 2002 October 27, when the planet was just out of the secondary eclipse, with the orbital phase $11.0^\circ \lesssim \alpha \lesssim 33.9^\circ$. A detailed description of the observations and data reduction to obtain one-dimensional spectra can be found in Winn et al. (2004) and Narita et al. (2005). The wavelength coverage of the spectra analyzed is from 554 nm to 681 nm, with a spectral resolution of $R \approx 45000$. The typical exposure time was 500 sec, and the S/N per pixel was ~ 350 .

The reasons for adopting exposure phases in the vicinity of the secondary eclipse, but not extremely close to it, are two fold. First, the strong back scattering of aerosol clouds or grains, if any, could dramatically brighten the planet. Second, we should not observe too close to either the primary transit or the secondary transit, because during those events the planet’s motion is nearly in the plane of the sky and its relative radial velocity variation is small, causing the scattered absorption lines to be blended with the direct absorption lines. For the HD 209458 data analyzed here, the velocity offsets between the stellar lines and their scattered counterparts is in the range of $27 - 80 \text{ km s}^{-1}$, sufficient to avoid blending in all cases.

The one-dimensional spectra are first normalized. We fit an 11th-order-spline3 function to obtain the blaze function of each order separately, and then merge the blaze functions of all the orders. The un-normalized spectra of each order are also merged in the same way and divided by the merged blaze function. Spectra are re-sampled and dispersion-corrected to logarithmically spaced bins

TABLE 1
PHYSICAL PARAMETERS OF THE SYSTEM HD209458 FROM
KNUTSON ET AL. (2007).

Parameter	Value and references
Mass of the star: $M_\star (M_\odot)$	$1.101^{+0.066}_{-0.062}$
Radius of the star: $R_\star (R_\odot)$	$1.125^{+0.020}_{-0.023}$
Mass of the planet: $M_P (M_J)$	0.64 ± 0.06
Radius of the planet: $R_P (R_J)$	$1.320^{+0.024}_{-0.025}$
Orbital inclination: i (degrees)	$86.929^{+0.009}_{-0.010}$
Orbital period: P_{orb} (days)	$3.52474859 \pm 0.00000038$
Transit epoch: T_0 (HJD)	$2,452,826.628521 \pm 0.000087$

after merger. All exposures are normalized separately, as their blaze functions vary due to instrumental variations (Winn et al. 2004; Narita et al. 2005). We note that the method to be discussed in Section 3.3 is also applicable to the un-normalized spectra. The normalization however simplifies the EW test to be described in Section 3.4. The reason we use an 11th-order-spline3 function for the fitting is to remove the large-scale profiles of the spectra without diluting the weak lines containing the scattered light signal.

We adopt the physical parameters of the system HD 209458 from Knutson et al. (2007), as summarized in Table 1, along with the Modified Julian Day (MJD) at the central time of each exposure, to predict $V_P(\phi)$.

3.3. Strategy I: Summing Scattered Light Lines

In this section, we search for the scattered light by aligning and combining the imprinted signals over a large set of stellar absorption lines as well as over exposures. The scattered signals are aligned by Doppler-shift correcting each exposure according to the corresponding $V_P(\phi)$. We also make a set of reference spectra by combining the same set of exposures, which, on the other hand, are Doppler-shift corrected with the $V_P(\phi)$ of another exposure. Therefore, extra absorptions around the predicted scattered-light centers would indicate a detection.

3.3.1. Details of the Strategy-I Procedure

First, 33 pre-processed spectra $S_{\log\lambda}^0$ are Doppler-shift corrected according to their predicted corresponding radial velocities. We use a logarithmic wavelength scale, and the super script “0” to refer to the star’s rest frame and “Z” for the planet’s. Then the shifted spectra, $S_{\log\lambda}^Z$, are corrected to have the same dispersion as that of $S_{\log\lambda}^0$. Here and throughout this study, spectra are always corrected to this standard dispersion after being shifted.

Second, a set of suitable stellar absorption lines were selected according to the following criteria: 1 - The line’s full-width at half-maximum (FWHM) must be larger than the threshold value $\text{FWHM}_{th} = 0.15\text{\AA}$, a value chosen by experimentation to maximize sensitivity. (The final result is, however, rather insensitive to the exact value of FWHM_{th} .) 2 - The line’s blue¹-ends extending to a wavelength range, which corresponds to the largest

¹ Due to the planet’s phases, its scattered spectra in all the 33 exposures we used in this study would be blue-shifted relative to the stellar spectra.

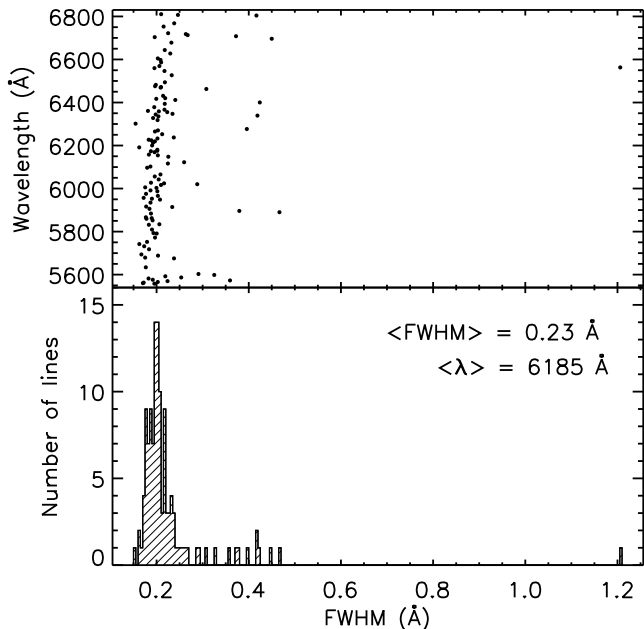


FIG. 1.— The 123 selected stellar absorption lines. Wavelength versus FWHM (*top*), and the distribution of FWHM (*bottom*).

radial velocity among all the exposures, needs to be relatively free of strong stellar lines. This is required to avoid contamination of any detection by strong stellar lines. The wavelengths of selected lines and the distribution of their FWHMs are displayed in Figure 1.

Third, small fragments ($\Delta\lambda \approx 1.7 \text{ Å}$ each²) of the spectra are averaged together, centering on the predicted scattered features and over all the selected lines and exposures. The combined normalized counts as a function of wavelength difference (from the predicted line centers) can be written as

$$C^Z(k) = \frac{1}{N_e N_l} \sum_{e=1}^{N_e} \sum_{l=1}^{N_l} S^{Z_e} [\log(\lambda_{k,el}) - \log(\lambda_{0,el})], \quad (4)$$

where $k = -50, -49, \dots, 49, 50$, and represents the k -th pixel on the bluer (redder) side of the scattered-light center ($k = 0$), if k is negative (positive); $\log(\lambda_{k+1,el}) - \log(\lambda_{k,el})$ corresponds to $d\lambda \approx 0.017 \text{ Å}$, i.e., the wavelength pixel size on the detector at the center of the spectral coverage³; $N_e = 33$ is the number of exposures, whereas $N_l = 123$ is the number of selected stellar absorption lines. Z_e stands for the “redshift” of the e^{th} exposure, and S^{Z_e} denotes the spectrum that has been Doppler-shift corrected according to the radial velocity of the e^{th} exposure. Wavelength solutions of different exposures agree with each other to within $\sim 0.03 \text{ Å}$, therefore the central wavelength of each stellar line, $\lambda_{0,el}$, is a function of both line and exposure. We account for the small variations in wavelength solutions by localizing each line in each exposure separately. In other words, $C^Z(k)$ is simply the average scattered spectral line generated by summing, after continuum normalization, over all of the selected lines (123 for our HD 209458 data) and all of the exposures (33 for our HD 209458 data), a total of

² $\Delta\lambda \approx 1.7 \text{ Å}$ was chosen to be big enough to cover several typical stellar line widths.

³ The actual spectral resolution at this point is $\approx 0.14 \text{ Å}$, equivalent to just about 8 detector pixels.

$N_e \times N_l$ separate spectral fragments (4059 in the case of the present data).

Fourth, we take the mean (as well as the median) values calculated from the same 33 pre-processed spectra, Doppler-shift corrected using N sets of scrambled redshifts (hereafter, reference spectra, for short), as the standard to compare $C^Z(k)$ with. This spectrum can be regarded as the “continuum” level, i.e., relatively free of scattered signals, and is given by

$$\langle C^{Z'}(k) \rangle = \frac{1}{N} \sum_{n=1}^N C^{Z'_n}(k), \quad (5)$$

where $C^{Z'_n}(k) = \frac{1}{N_e N_l} \sum_{e=1}^{N_e} \sum_{l=1}^{N_l} S^{Z'_{n,e}} [\log(\lambda_{k,el}) - \log(\lambda_{0,el})]$. $\{Z'_{n,e}\}$ is a permutation of $\{Z_e\}$, and there are $N = 1,000$ sets of random permutations. We note it is essential that $\{Z'_{n,e}\}$ is a permutation of $\{Z_e\}$, rather than purely random redshifts, because using a permutation of $\{Z_e\}$ ensures the exact same fragments of stellar spectra go into $C^{Z'_n}(k)$, as those in $C^Z(k)$.

Fifth and finally, we define the combined scattered signal as the residual given by

$$\Delta C(k) \equiv C^Z(k) - \langle C^{Z'}(k) \rangle. \quad (6)$$

Given scattered light, $\Delta C(k)$ will be negative around $k = 0$, with a profile similar to the combined stellar lines scaled by $\epsilon(\alpha, \lambda)$. Strictly speaking, $\langle C^{Z'}(k) \rangle$ is affected to some degree by the scattered-light signal, even though the redshifts have been scrambled. This is because occasionally the randomly assigned redshift will happen to be or close to the appropriate redshift of the exposure. Therefore $\langle C^{Z'}(k) \rangle$ serves as a lower limit for the true continuum level, and $\Delta C(k)$ yields a conservative value.

3.3.2. Results for Strategy I

Figure 2 shows the normalized count $C(k)$ and the residual $\Delta C(k)$ obtained from analyzing the Subaru/HDS spectra of HD 209458b. The overall shape of $C(k)$ is a result of the combination of multiple stellar spectrum segments. The significance levels plotted in (A), as well as the $1\text{-}\sigma$ errors shown in (B) are calculated from the variance among the reference spectra. $\Delta C(k)$ along with the $1\text{-}\sigma$ errors in (C) and (D) are from the jackknife- and bootstrap- re-samplings (re-sampled over both lines and exposures) of the data along with the corresponding reference spectra, respectively. The re-sampling tests produced similar errors to those solely estimated from the variations in reference spectra. To test the algorithms, we also analyzed a mock/simulated spectrum, obtained by combining the same set of stellar lines scaled by a factor of 1.2×10^{-4} . This simulated signal indicates the expected scattered light assuming a planet-to-star flux ratio of $\epsilon = 1.2 \times 10^{-4}$. The comparison of the observations and simulated signal shown in Figure 2 is intriguing in that the data are consistent with a low statistical significance detection of the scattered light, with $\epsilon \gtrsim 10^{-4}$ at the $1\text{-}\sigma$ level, as the data follow the simulated signal tantalizingly well, especially around the predicted line center where the signal should be the strongest.

Figure 3 also displays the normalized residual counts $\Delta C(k)$, but in this figure the actual spectral resolution,

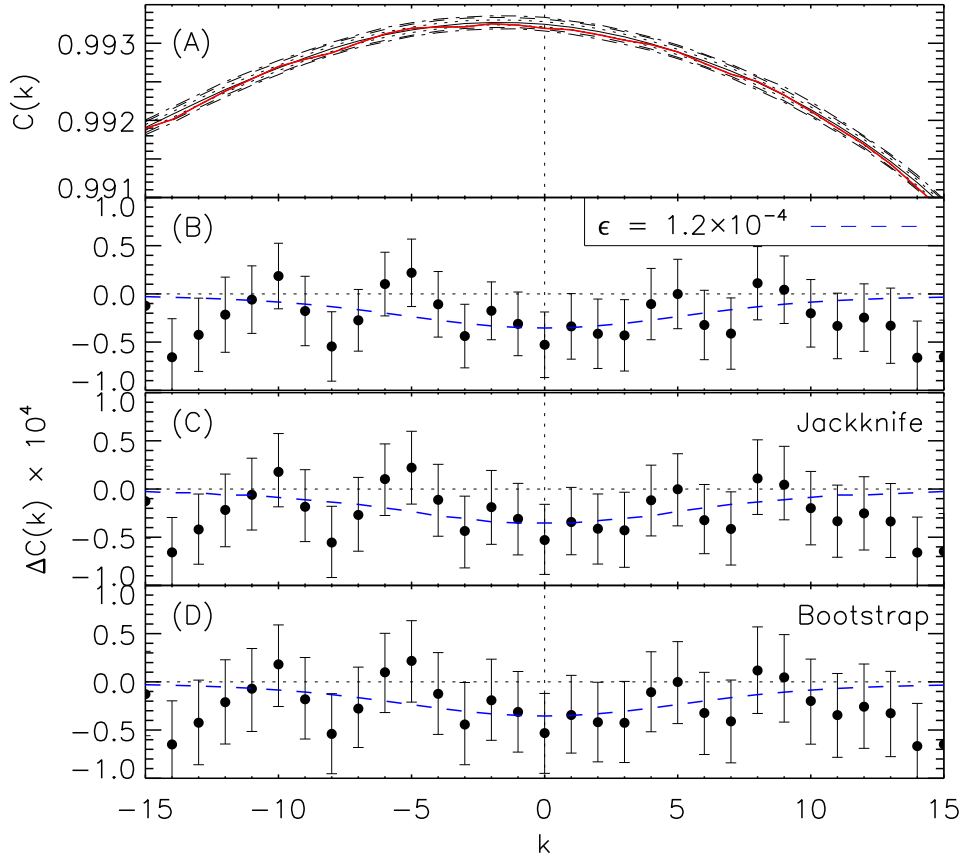


FIG. 2.— The normalized count $C(k)$ and the residual $\Delta C(k)$ as a function of wavelength difference k , relative to the predicted scattered line’s center, aligned and average-combined over a large set of stellar lines and over exposures. Each exposure has been Doppler-shift corrected to align the scattered signals, according to the planet’s relative radial velocity to the star. (A): the red curve shows $C^Z(k)$, whereas the black curves represent the median (*solid*; also same as the mean), and 68% (*dotted*), 95% (*dashed*), and 99% (*dash-dotted*) significance levels, obtained from 1,000 sets of scrambling-shifted spectra ($\{C^{Z_n}(k)\}$); (B), (C) and (D): the black filled-circles show the residual $\Delta C(k)$, which is the difference between $C^Z(k)$ (*red*) and $\langle C^{Z_n}(k) \rangle$ (*black-solid*). Results from the simulated scattered light by combining the stellar lines scaled by a factor of 1.2×10^{-4} are shown as *blue-dashed* curves. The error bars in (B) correspond to 1σ -errors obtained from the significance levels shown in (A), whereas (C) and (D) present the results of 4,059 sets of jackknife- and bootstrap-re-samplings. In all the panels, one pixel corresponds to $\sim 0.017\text{\AA}$, the approximate size of a detector pixel, about one eighth of the actual spectral resolution. The systematic decrease in $\Delta C(k)$ at more than 12 pixels to the red or blue of the line center is due to the influence of stellar absorption lines beyond the edges of the region chosen to be clear of such interference.

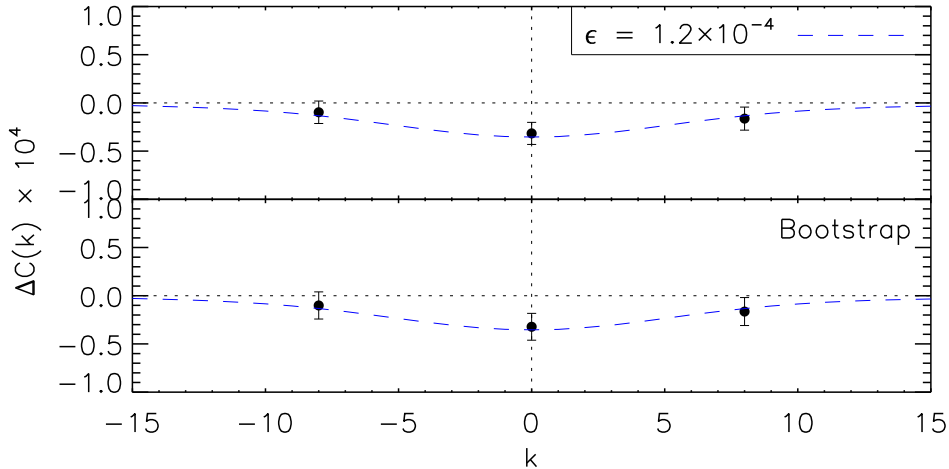


FIG. 3.— The normalized residual counts $\Delta C(k)$ as a function of wavelength difference k , as in panels (B) and (D) of the previous figure, but in this case the data points have been rebinned by a factor of 8. This corresponds to the true spectral resolution of the data, rather than to the detector pixel size. The rebinnig is arranged such that the predicted line center position at $k = 0$ is in the middle of the central point. The dashed line shows the expected shape of the composite scattered light line assuming a 1.2×10^{-4} scattered light fraction.

about 8 detector pixels, is used. There are thus only three points across the expected composite scattered light absorption line, but the error bars are correspondingly reduced, and the points are not strongly correlated by the finite spectral resolution as they are in Figure 2. Since the two figures simply display the same data at two different wavelength resolutions, they are both naturally consistent with the same scattered-light fraction of 1.2×10^{-4} and the same line shape, shown by the *blue-dashed* line.

3.4. Strategy II: Equivalent Width Ratio Distributions

In this section, we further suggest a method to measure the planet-to-star flux ratio ϵ by examining the distribution of the EW ratios between the scattered and the stellar absorption lines, measured for a large set of lines and exposures. The FWHMs of stellar lines displayed in Figure 1 are used to set the wavelength range over which the EWs of both stellar and scattered lines are evaluated. Since this method effectively concentrates all of the “missing flux” signal into a single number with appropriate weighting of the stronger and weaker features, we would expect better sensitivity performance than Strategy I. The cost, of course, is loss of all information about the shape of the composite shape of the scattered lines and thus of a useful check that the measured feature has the expected character of scattered light. The two approaches are thus complementary.

3.4.1. Details of the Strategy-II Procedure

We adopt a dimensionless EW, which is convenient for a logarithmically linear wavelength scale, given by

$$W \equiv \int \frac{d\lambda}{\lambda_0} \left[1 - \frac{S_\lambda}{S(0)} \right] = \ln 10 \cdot \int \left[1 - \frac{S_{\log \lambda}}{S(0)} \right] d \log \lambda, \quad (7)$$

where λ_0 is the central wavelength of a stellar absorption line and $S(0)$ denotes its local continuum. In logarithmically linear wavelength scale, W can be discretized as

$$W = A \cdot \sum_i \left[1 - \frac{S_{\log \lambda_i}}{S(0)} \right], \quad (8)$$

where $A \equiv \ln 10 \cdot \Delta \log \lambda$ is a constant, and the summation goes over all pixels inside a wavelength range of twice that of the line’s FWHM and centered at λ_0 . Since different stellar lines have different FWHMs as shown in Figure 1, a variable number of pixels are included in the EW integrations by making use of the line-strength information, whereas in Strategy I, the same number of pixels are combined for all lines.

The EW of the stellar lines, $W_{e,l}^* = A \cdot \sum_i [1 - S_{\log \lambda_{i,el}}^0 / S_{e,l}^0(0)]$, is calculated for each line (denoted by l) in each exposure (denoted by e), using the stellar FWHMs measured in the initial exposure, which are shown in Figure 1. To check for FWHM variability, we measure the FWHMs in both the initial and final exposures and find that they agreed within 0.1 per cent.

For each line, the local continuum $S_{e,l}^0(0)$ is estimated by averaging the median of the counts in two spectral intervals on either side of the line, with a size chosen to be neither too large to reflect the local continuum level nor too small for accurate statistics. We use a range of 50 pixels, corresponding to ~ 1 Å. The results have been tested to be independent of the adopted size of the range over which the continuum levels are estimated.

For the scattered signals, $W_{e,l}^{Z_e} = A \cdot \sum_i [1 - S_{\log \lambda_{i,el}}^{Z_e} / S_{e,l}^{Z_e}(0)]$, where the super script Z_e represents the spectrum S has been Doppler-shift corrected with the Doppler shift of the e^{th} exposure. We use the FWHMs of the stellar lines, assuming that the scattered light is a replica of starlight, scaled by a factor of ϵ . The local continuum $S_{e,l}^{Z_e}(0)$ is taken as the median of the line’s blue end, since the red end often overlaps the associated strong stellar lines. The EW ratio is then given by $R_{e,l}^{Z_e} \equiv W_{e,l}^{Z_e} / W_{e,l}^*$. The EW-ratio measurements of N_l lines in N_e exposures constitute a statistical sample of $\{R_{e,l}^{Z_e}\}$, which has $N_l \times N_e$ data points.

We also calculate $\{R_{e,l}^{Z'_n}\}$ for N sets of reference spectra, to construct a standard comparison pool. Both mean and median are adopted as statistical measures, where $M(R^Z)$ denotes taking either the mean or the median of $\{R_{e,l}^{Z_e}\}$. Finally, we define the residual EW ratio, given by

$$\Delta M(R) \equiv M(R^Z) - \langle M(R^{Z'}) \rangle, \quad (9)$$

where $\langle M(R^{Z'}) \rangle = \frac{1}{N} \sum_{n=1}^N M(R^{Z'_n})$,

is the comparison standard obtained from N sets of scrambling-shifted reference spectra. Given null (by construction) reference-spectrum signal, $\Delta M(R)$ will be positive and give a direct estimate of ϵ .

3.4.2. Results for Strategy II

Figure 4 shows $\Delta M(R)$ for both the median and the mean statistics, obtained from the HD 209458b data, simulated scattered signals, reference spectra, and bootstrap re-samplings. We have also generated jackknife re-samplings, which produced similar results to those of the bootstrap re-samplings, and both re-sampling analysis yield consistent errors with those estimated from the variation of reference spectra. To test the linearity of the algorithm, we injected mock/simulated scattered signals, assuming $\epsilon = 10^{-4}$ and 2×10^{-4} , respectively. The injected signals are recovered linearly through the data pipeline as expected, since our algorithm only involves linear transformations. These EW-ratio results suggest $\epsilon = (1.4 \pm 2.9) \times 10^{-4}$ ($(3.6 \pm 2.0) \times 10^{-4}$), according to the median (mean) statistics. The mean is more sensitive to outliers which can be caused by stellar-line overlaps or inaccurate estimation of the local continuum levels, or by real intrinsic variation of the albedo with wavelength or phase, whereas the median should be more robust and representative of a global effective albedo over the whole wavelength and phase ranges.

4. SUMMARY AND DISCUSSION

We have developed a simple, robust, linear, and model-independent technique to detect scattered starlight from transiting CEGPs, by measuring scattered spectral features at predictable Doppler shifts from the stellar lines due to planets’ orbital motions. There are two main variations of this technique. First, spectrum fragments have been aligned and combined over a large set of stellar absorption lines as well as over many exposures taken near the secondary eclipse. Second, the planet-to-star flux ratio has been determined by examining the distribution

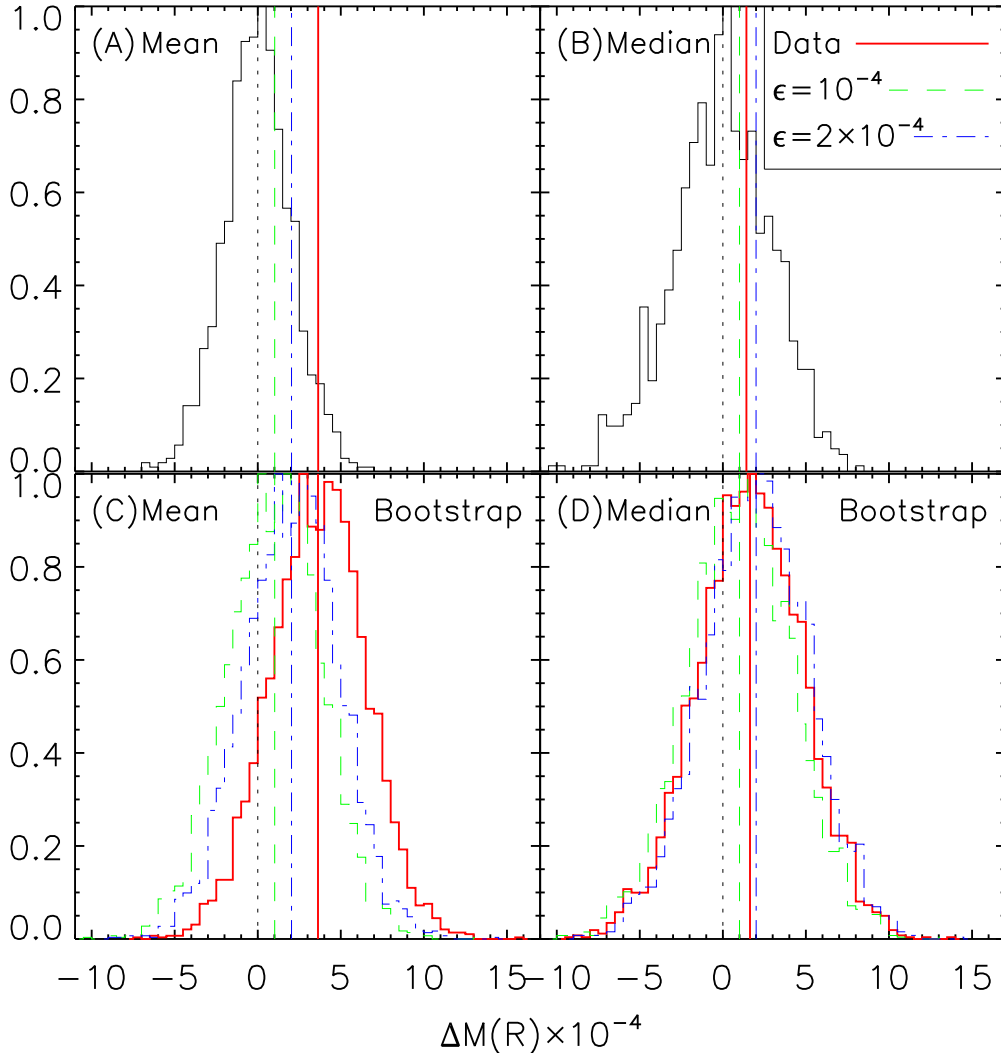


FIG. 4.— The EW ratio $\Delta M(R)$. (A) and (C) show the mean results whereas (B) and (D) present the median. In (A) and (B), the histogram displays the normalized distribution of results from 1,000 sets of scrambling-shifted spectra. The dotted line represents the averages of the distributions. As shown by the legend in (B), the other three vertical lines show results calculated from the data (thick red-solid), the simulated scattered-light spectra assuming $\epsilon = 10^{-4}$ (thin green-dashed), and $\epsilon = 2 \times 10^{-4}$ (thin blue-dash-dotted), respectively. (C) and (D) show the normalized distributions of results from 4,059 bootstrap-re-samplings, for the data (thick red-solid), the simulated scattered-light spectra assuming $\epsilon = 10^{-4}$ (thin green-dashed), and $\epsilon = 2 \times 10^{-4}$ (thin blue-dash-dotted), respectively. The three vertical lines mark the averages of the normalized distributions. $\Delta M(R) = 0$ is also shown as dotted lines for comparison.

of the EW ratios between the scattered and stellar absorption lines. We have made a comparison sample by Doppler-shift correcting the exposures with multiple sets of scrambled, instead of the real, redshifts. This comparison sample has been passed through the same data pipeline, and provided the control comparisons, as well as the significance levels of any detections. Jackknife- and bootstrap-re-samplings have yielded consistent errors with those determined from the variations of the reference spectra. We have also produced spectra with simulated scattered signals, using the stellar absorption lines scaled by a factor of an assumed planet-to-star flux ratio. The simulated signals have been fully recovered through the data pipeline. Physical parameters of the system are required to have been determined, in order to predict the planet's relative radial velocity at each orbital phase, and further localize its imprinted signals

on the recorded spectra. These parameters can be determined from radial-velocity and photometric observations of transiting CEGPs with high precision and reliability.

As a case study, we have analyzed very high S/N optical spectra of HD 209458b, acquired with the Subaru HDS in UT 2002 October. Our results suggest an average planet-to-star flux ratio of $(1.4 \pm 2.9) \times 10^{-4}$, in the wavelength from 554 nm to 681 nm, when the planet was during the orbital phases $11.0^\circ < \alpha < 33.9^\circ$. Assuming a Lambert-sphere phase function (Pollack et al. 1986; Charbonneau et al. 1999), the equivalent geometric albedo can be estimated as 0.8 ± 1.6 , according to Equation 3, where we take the phase of the middle exposure $\phi \approx 0.561$, corresponding to $\alpha = 22.3^\circ$, out of $11.0^\circ < \alpha < 33.9^\circ$ for all the exposures we used. The best previous existing constraint on scattered light from HD 209458b is based on direct imaging with the

MOST satellite (Rowe et al. 2006). Rowe et al. (2006) found a $1\text{-}\sigma$ limit on the planet-to-star flux ratio of 4.88×10^{-5} , corresponding to a geometric albedo upper limit in *MOST* bandpass (400-700 nm) of 0.25. Our results provide a useful point of comparison for this difficult measurement, covering a somewhat different wavelength range and based on different observational strategies and analysis techniques.

These results do not seem yet able to support a comparison to models of the HD 209458b atmosphere or to justify detailed physical interpretation, but they do not miss the mark by far and are thus quite encouraging. Specifically, the Subaru HDS data analyzed here constitute well under 5 hours of total exposure time; it would be possible to obtain more data, and there is no indication in the present data of systematic problems (such as instrumental instabilities) that would prevent further integration from producing a greater sensitivity. Moreover,

one significantly more favorable transiting CEGP system (HD 189733) is known, and others may be discovered. In combination with measurements of re-emitted thermal radiation (e.g. Charbonneau et al. 2005), scattered light studies offer the possibility of major qualitative advances in our understanding of CEGPs, a central riddle in the study of exoplanets generally.

This work is based on data from the Subaru Telescope, which is operated by the National Astronomical Observatory of Japan. We wish to recognize and acknowledge the very significant cultural role and reverence that the summit of Mauna Kea has always had within the indigenous Hawaiian community. We are most fortunate to have the opportunity to conduct observations from this mountain.

REFERENCES

- Brown, T. M., Charbonneau, D., Gilliland, R. L., Noyes, R. W., & Burrows, A. 2001, *ApJ*, 552, 699
- Burrows, A., Hubeny, I., & Sudarsky, D. 2005, *ApJ*, 625, L135
- Cameron, A. C., Horne, K., Penny, A., & James, D. 1999, *Nature*, 402, 751
- Charbonneau, D., Allen, L. E., Megeath, S. T., Torres, G., Alonso, R., Brown, T. M., Gilliland, R. L., Latham, D. W., Mandushev, G., O'Donovan, F. T., & Sozzetti, A. 2005, *ApJ*, 626, 523
- Charbonneau, D., Brown, T. M., Latham, D. W., & Mayor, M. 2000, *ApJ*, 529, L45
- Charbonneau, D., Noyes, R. W., Korzennik, S. G., Nisenson, P., Jha, S., Vogt, S. S., & Kibrick, R. I. 1999, *ApJ*, 522, L145
- Chauvin, G. 2007, in Proceedings of the conference In the Spirit of Bernard Lyot: The Direct Detection of Planets and Circumstellar Disks in the 21st Century. June 04 - 08, 2007. University of California, Berkeley, CA, USA. Edited by Paul Kalas., ed. P. Kalas
- Collier Cameron, A., Horne, K., Penny, A., & Leigh, C. 2002, *MNRAS*, 330, 187
- Henry, G. W., Marcy, G. W., Butler, R. P., & Vogt, S. S. 2000, *ApJ*, 529, L41
- Knutson, H. A., Charbonneau, D., Noyes, R. W., Brown, T. M., & Gilliland, R. L. 2007, *ApJ*, 655, 564
- Leigh, C., Cameron, A. C., & Guillot, T. 2003, *MNRAS*, 346, 890
- Marley, M. S., Gelino, C., Stephens, D., Lunine, J. I., & Freedman, R. 1999, *ApJ*, 513, 879
- Mayor, M. & Queloz, D. 1995, *Nature*, 378, 355
- Mazeh, T., Naef, D., Torres, G., Latham, D. W., Mayor, M., Beuzit, J.-L., Brown, T. M., Buchhave, L., Burnet, M., Carney, B. W., Charbonneau, D., Drukier, G. A., Laird, J. B., Pepe, F., Perrier, C., Queloz, D., Santos, N. C., Sivan, J.-P., Udry, S., & Zucker, S. 2000, *ApJ*, 532, L55
- Narita, N., Suto, Y., Winn, J. N., Turner, E. L., Aoki, W., Leigh, C. J., Sato, B., Tamura, M., & Yamada, T. 2005, *PASJ*, 57, 471
- Noguchi, K., Aoki, W., Kawanomoto, S., Ando, H., Honda, S., Izumiura, H., Kambe, E., Okita, K., Sadakane, K., Sato, B., Tajitsu, A., Takada-Hidai, T., Tanaka, W., Watanabe, E., & Yoshida, M. 2002, *PASJ*, 54, 855
- Perryman, M. A. C. 2000, *Reports of Progress in Physics*, 63, 1209
- Pollack, J. B., Rages, K., Baines, K. H., Bergstralh, J. T., Wenkert, D., & Danielson, G. E. 1986, *Icarus*, 65, 442
- Rowe, J. F., Matthews, J. M., Seager, S., Kuchnig, R., Guenther, D. B., Moffat, A. F. J., Rucinski, S. M., Sasselov, D., Walker, G. A. H., & Weiss, W. W. 2006, *ApJ*, 646, 1241
- Seager, S. & Sasselov, D. D. 1998, *ApJ*, 502, L157+
- Seager, S., Whitney, B. A., & Sasselov, D. D. 2000, *ApJ*, 540, 504
- Sudarsky, D., Burrows, A., & Hubeny, I. 2003, *ApJ*, 588, 1121
- Sudarsky, D., Burrows, A., & Pinto, P. 2000, *ApJ*, 538, 885
- Winn, J. N., Suto, Y., Turner, E. L., Narita, N., Frye, B. L., Aoki, W., Sato, B., & Yamada, T. 2004, *PASJ*, 56, 655